The Influence of Atmospheric Rivers over the South Atlantic on Winter Rainfall in South Africa

R. C. BLAMEY

Department of Oceanography, University of Cape Town, Rondebosch, South Africa

A. M. RAMOS, R. M. TRIGO, AND R. TOMÉ

Instituto Dom Luiz, Faculdade de Ciências, Universidade de Lisboa, Lisbon, Portugal

C. J. C. REASON

Department of Oceanography, University of Cape Town, Rondebosch, South Africa

(Manuscript received 15 June 2017, in final form 6 October 2017)

ABSTRACT

A climatology of atmospheric rivers (ARs) impinging on the west coast of South Africa (29°–34.5°S) during the austral winter months (April–September) was developed for the period 1979–2014 using an automated detection algorithm and two reanalysis products as input. The two products show relatively good agreement, with 10–15 persistent ARs (lasting 18 h or longer) occurring on average per winter and nearly two-thirds of these systems occurring poleward of 35°S. The relationship between persistent AR activity and winter rainfall is demonstrated using South African Weather Service rainfall data. Most stations positioned in areas of high topography contained the highest percentage of rainfall contributed by persistent ARs, whereas stations downwind, to the east of the major topographic barriers, had the lowest contributions. Extreme rainfall days in the region are also ranked by their magnitude and spatial extent. The results suggest that although persistent ARs are important contributors to heavy rainfall events, they are not necessarily a prerequisite. It is found that around 70% of the top 50 daily winter rainfall extremes in South Africa were in some way linked to ARs (both persistent and nonpersistent). Overall, the findings of this study support similar investigations on ARs in the North Atlantic and North Pacific.

1. Introduction

The southwest region of South Africa is the only part of the country that receives most of its rainfall during the austral winter months (May–September). It is an extremely heterogeneous climate region, with areas ranging from semiarid to relatively wet on the windward slopes of the mountains. This heterogeneity is due to a number of factors, such as its geographic location, the complex topography that extends across large stretches of the region, and the neighboring cold, upwelled waters along the west coast with warmer waters along the southern coast (Agulhas Current). Located within this region is the city of Cape Town, the second-largest metropolitan municipality in South Africa, with around 3.7 million inhabitants (based on a 2011 census). Cape Town is completely reliant on the winter rainfall as a primary water source, both for drinking and for the treatment of sewerage and wastewater. The main water supply is stored in numerous dams within the Cape Fold Mountains located to the east of the city (see Fig. 1). These mountains can be described as "water towers" (Liniger et al. 1998; Messerli et al. 2004). They contribute considerably to the total local discharge and are one of the key water sources for South Africa (WWF 2013).

Poor winter rainfall can often have dire consequences for Cape Town and the surrounding areas, particularly when it occurs over successive years and results in severe water restrictions being put in place (e.g., 2003–04 and 2015–17). Despite the importance of the winter rainfall to the local population and the economy (e.g., agriculture), relatively little is understood regarding the main drivers/processes behind the interannual variability, compared to those behind the summer rainfall region of

Corresponding author: Ross Blamey, ross.blamey@uct.ac.za

DOI: 10.1175/JHM-D-17-0111.1

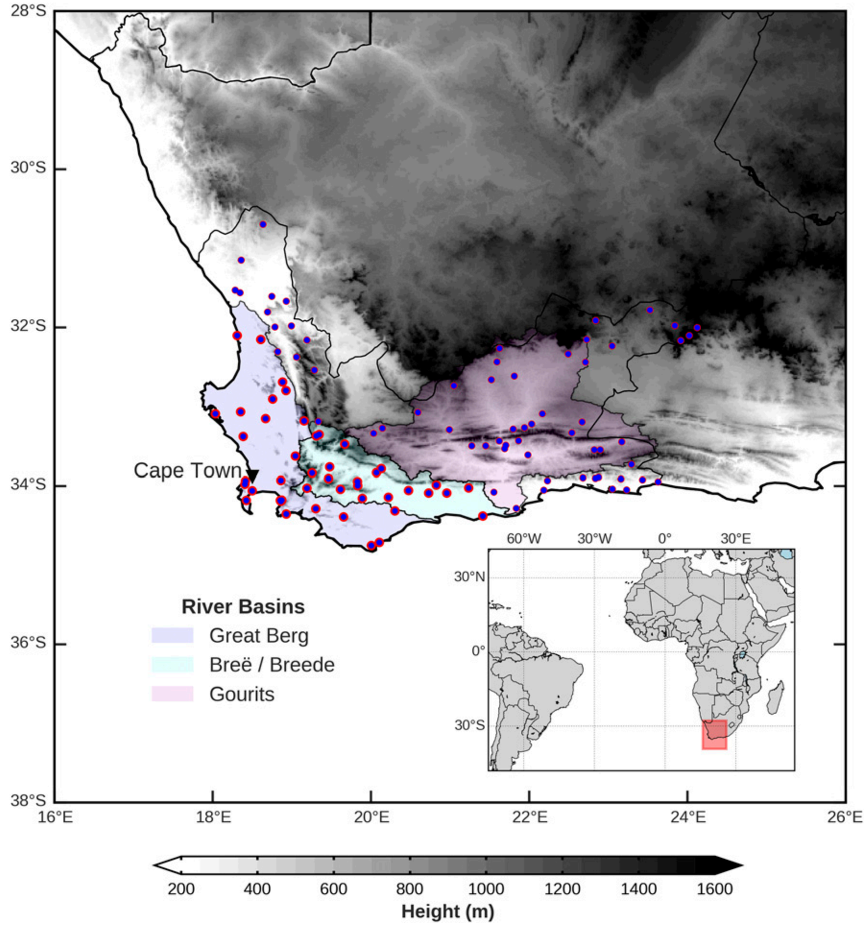

FIG. 1. Topography (gray shading; m MSL) of the west coast of South Africa, location of SAWS stations (magenta/purple dots), and the spatial distribution of the three key river basins (color shading) within the Western Cape province of South Africa. Only stations that fall within the Great Berg and Breede River basins are used in the analysis (denoted by larger circles).

the country. There is also limited information regarding the nature of regional extreme rainfall events, which can cause significant damage and sometimes loss of life. Midgley et al. (2007) estimated that a series of extreme rainfall events in the winter rainfall region during 2003–07 resulted in damage of an accumulated value of around $100 million.

Winter rainfall in South Africa is typically produced via cold fronts and associated extratropical cyclones, while other westerly disturbances, such as cutoff lows, may occasionally also produce considerable rainfall over the region (e.g., Singleton and Reason 2007a,b). Interannual variability in the winter rainfall has been linked to numerous large-scale modes of variability, which include El Niño–Southern Oscillation (Philippon et al. 2012) and the southern annular mode (Reason and Rouault 2005). Regional anomalies in Antarctic sea ice extent (Blamey and Reason 2007) and sea surface temperature in the South Atlantic (Reason 1998; Reason et al. 2002; Reason and Jagadheesha 2005) have also been identified as features influencing local rainfall patterns, and intraseasonal teleconnections with convection over South America may exist as well (Grimm and Reason 2015). However, a comprehensive understanding of the drivers behind the winter rainfall remains elusive, and thus, improving the predictability of the local winter rainfall is a significant scientific challenge.

An important question not hitherto investigated for South Africa is whether atmospheric rivers (ARs) can make a significant contribution to rainfall, particularly to heavy rainfall events. Over the past decade, increasing attention has been paid to the important role ARs play in the water cycle, particularly in the midlatitudes. Transport of water vapor from the tropics to the midlatitudes is generally confined to four or five narrow regions around the world (Zhu and Newell 1998). Though these few narrow corridors only take up 10% of the circumference of the Earth at that latitude, they are thought to channel around 90% of the total volume of water vapor poleward (Zhu and Newell 1998). These corridors are composed of filamentary bands of intense, vertically integrated water vapor transport, commonly referred to as ARs (Newell et al. 1992; Zhu and Newell 1998).

ARs appear to be dynamically linked with the development and movement of extratropical cyclones, with most of the moisture flux confined to the lower atmosphere and aligned along or ahead of cold fronts associated with extratropical cyclones (Ralph et al. 2004). Thus, climatologically, there are generally more ARs during the winter months compared to the summer months because of the strong association between ARs and midlatitude/extratropical cyclones (Gimeno et al. 2014). However, there is still debate over how these rivers or narrow corridors of high water vapor form, with some research asserting that high water vapor content is achieved through direct moisture transport from the tropics (Ralph et al. 2004; Wick et al. 2013; Neiman et al. 2013; Rutz et al. 2014). Alternatively, results by Bao et al. (2006) and Dacre et al. (2015) indicate that ARs are not necessarily fed by long-distance moisture transport from the tropics/subtropics (as implied by the word "river"), but are rather the result of local sources of water vapor exported from extratropical cyclones as they travel poleward. Ramos et al. (2016) show, through a Lagrangian analysis of the main moisture sources of the ARs that make landfall on the western European coast, that the anomalous moisture linked with the ARs comes mainly from subtropical areas and, to a lesser extent, from the midlatitudes. A small anomalous moisture source was also identified from within the tropics.

Although there is some debate about the formation of ARs, there is mounting evidence that these features play an important role in heavy rainfall events in midlatitude regions, such as western North America (e.g., Ralph et al. 2006; Dettinger et al. 2011; Warner et al. 2012) and the central United States (e.g., Moore et al. 2012). A global overview of the preferred location of ARs and their associated landfall frequency is provided by Gimeno et al. (2016). Given the strong water vapor content and low static stability, ARs have the potential to produce heavy rainfall, particularly in regions with strong topography (Neiman et al. 2002; Ralph et al. 2004; Rutz et al. 2014). Over the 1998–2005 period, nearly every major flooding event of the Russian River in California was associated with an AR (Ralph et al. 2006; Ralph and Dettinger 2012). Dettinger et al. (2011) advocate that extreme rainfall events (3-day rainfall totals exceeding 40 cm) associated with landfalling ARs in California are historically comparable, in magnitude and frequency, to regions in the southeastern United States associated with landfalling hurricanes and tropical storms. Extreme rainfall events linked to ARs are not limited to the United States; cases have also been documented in Great Britain (Lavers et al. 2011, 2012), along the west coast of continental Europe (Lavers et al. 2013; Ramos et al. 2015), in East Asia (Hirota et al. 2016), and in South America (Viale and Nuñez 2011). A number of historical extreme floods on the Iberian Peninsula have been linked with well-defined ARs over the North Atlantic Ocean, including the record 1909 flood of the Duero River (Pereira et al. 2016).

The importance of ARs is probably more evident from their contribution to overall rainfall totals. In North America, it has been found that ARs contribute anywhere between 20% and 45% of the rainfall in central and Northern California, even rising closer to 50% in some years (Dettinger et al. 2011). It is not just the west coast of North America that benefits from AR related rainfall; Lavers and Villarini (2015) found that ARs can produce similar contributions in parts of the central United States. These results are, however, month dependent, with greater contributions often taking place during the winter period. Similar results are documented for western Europe, with ARs contributing between 20% and 30% of all rainfall (Lavers and Villarini 2015). However, little research on ARs and their influence on regional rainfall patterns has been done outside the North Pacific or North Atlantic domains.

The objectives of this study are twofold: 1) to provide some insight into the location and frequency of ARs in a relatively poorly studied region (the South Atlantic) and 2) to better understand the role that such phenomena play in winter rainfall, including extreme rainfall events, across the winter rainfall region of South Africa (see Fig. 1 for location). Annual rainfall totals within southwest South Africa could potentially be dependent on not only the number of frontal systems per winter, but also on the intensity of the systems. Thus, a few large frontal events, fueled by ARs, could have a considerable impact on winter season rainfall totals and on the number of heavy rainfall events. Understanding the sources of moisture for winter rainfall and the mechanisms through which it is transported into the region will not only assist in improving seasonal weather forecasting, but may also provide much-needed information on the frequency and magnitude of extreme rainfall and flood events. This would ultimately benefit regional water management and local disaster mitigation activities.

2. Data and methodology

a. AR data sources

Depending on the application, ARs are typically identified by integrated water vapor (IWV) thresholds in satellite imagery, such as that provided by the Special Sensor Microwave Imager (SSM/I) (e.g., Neiman et al. 2008; Wick et al. 2013). However, a limitation of this particular data source is that it does not contain information about vertical wind profiles, and thus, it is unable to quantify actual water vapor transport. Instead, it can only indicate the presence of water vapor concentrations. Furthermore, gaps in the satellite swaths can hamper any automated AR identification procedure. Because of limitations in satellite data, other studies have used integrated water vapor transport (IVT) from reanalysis products for AR identification (e.g., Lavers et al. 2012; Rutz et al. 2014; Ramos et al. 2015). The primary advantage of using IVT is that it is more representative of the key characteristic (i.e., moisture transport) of ARs. Another argument for using IVT is that it is strongly related to precipitation over complex terrain (Junker et al. 2008; Ralph et al. 2013), and it captures the penetration of ARs farther inland (Rutz et al. 2014).

The AR detection methodology used by Lavers et al. (2012) and Ramos et al. (2015), discussed in the subsequent section, is applied here to two different reanalysis datasets, namely, the European Centre for Medium-Range Weather Forecast (ECMWF) interim reanalysis (ERA-Interim, hereafter ERAI) data (Dee et al. 2011) and the National Centers for Environmental Prediction (NCEP)–Department of Energy (DOE) Second Atmospheric Model Intercomparison Project (AMIP-II) reanalysis (hereafter NCEP-2) (Kanamitsu et al. 2002). ERAI and NCEP-2 are both available at 6-hourly time steps, centered on synoptic times (0000, 0600, 1200, and 1800 UTC) from 1979 to 2014. However, ERAI is provided at a relatively high resolution of 0.75°, while NCEP-2 has a lower horizontal resolution of 2.5°. The variables retrieved for both reanalyses were the specific humidity q and zonal u and meridional v winds at 1000, 925, 850, 700, 600, 500, 400, and 300 hPa. Only data covering the austral winter months (April–September) are used here. One of the advantages of using reanalysis products, rather than just a satellite product, is that they use data assimilation of observations to produce the best available three-dimensional dynamical representation of the atmosphere.

It has been recognized that the choice of reanalysis product and identification method used can influence the number of ARs identified in a given period (e.g., Lavers et al. 2012). Apart from differences in grid resolutions, this potential bias could partly be due to differences in reanalysis production methods (i.e., data-assimilating models used and the type of observations that are incorporated), which can lead to variations in the reanalyses (Rienecker et al. 2011; Trenberth et al. 2011). ERAI is one of the reanalysis products that assimilates data from the SSM/I water vapor channel (since 1987) (Dee et al. 2011) and has already been used in AR investigations in other regions, such as the North Pacific (e.g., Rutz et al. 2014) and North Atlantic (e.g., Lavers and Villarini 2015). The use of a high-resolution reanalysis product is an obvious choice, given the fine filament structure of ARs, and thus assists in the automated approach for identification and tracking. Although the earlier version of the NCEP reanalysis (NCEP–NCAR; Kalnay et al. 1996) is available for a longer period (1948–present), it is not used because of inhomogeneities in the data in the Southern Hemisphere prior to 1979 (Kanamitsu et al. 2002; Tennant 2004).

b. AR identification method

ARs have typically been defined or identified as plumes of moisture that are greater than 2000 km in length and less than 1000 km in width and contain an IWV content exceeding 20 mm (Ralph et al. 2004; Neiman et al. 2008; Dettinger et al. 2011). When compared to IWV, a single IVT threshold value for AR identification is not as well defined or widely used in the literature. Lavers et al. (2012) established a varying IVT threshold value through the use of percentiles in order to accommodate the various IVT distributions obtained over distinct pairs of latitude and longitude. This method results in different IVT thresholds being set for different regions around the world and for different reanalysis datasets. A similar approach is adopted in this study. The IVT is calculated from 1000 to 300 hPa in an Eulerian framework (e.g., Neiman et al. 2008; Lavers et al. 2012) as

$$\mathrm{IVT} = \sqrt{\left(\frac{1}{g}\int_{1000\,\mathrm{hPa}}^{300\,\mathrm{hPa}} qu\,dp\right)^2 + \left(\frac{1}{g}\int_{1000\,\mathrm{hPa}}^{300\,\mathrm{hPa}} qv\,dp\right)^2},$$

where q is the layer-averaged specific humidity (kg kg^{-1}); u and v are the layer-averaged zonal and meridional winds (m s^{-1}), respectively; g is the acceleration due to gravity; and dp is the pressure difference between two adjacent pressure levels.

The focus of this study is on ARs making landfall along the west coast of South Africa (see Fig. 2 for an example). Using the ERAI and NCEP-2 reanalysis data, ARs were identified based on the following steps:

1) Based on the work of Lavers et al. (2012), the 85th-percentile threshold of the maximum IVT was computed between 27.75° and 35.25°S (27.5°–35.0°S), along the reference meridian at 15°E, in

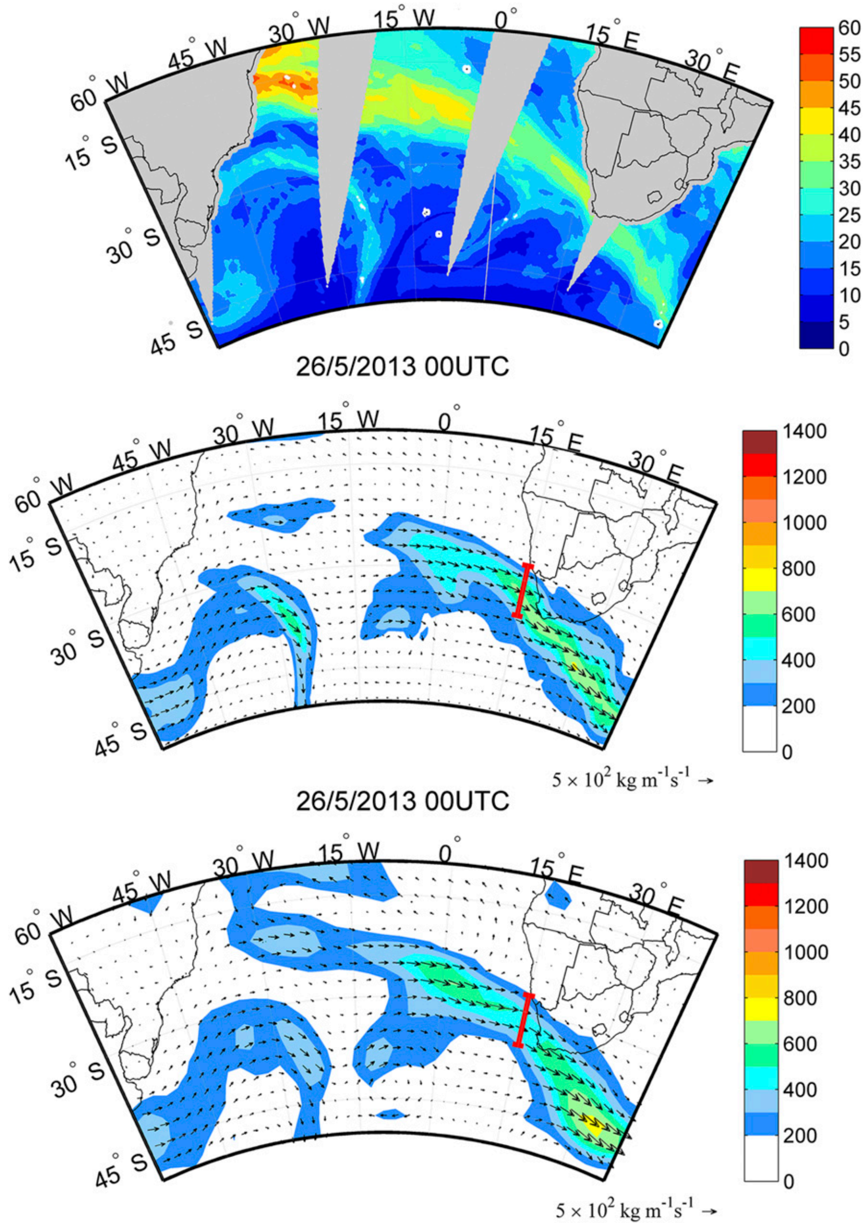

FIG. 2. An example of an AR impacting South Africa on 26 May 2013 in (top) SSM/I satellite data (morning passes), illustrating the IWV over the South Atlantic; (middle) the same AR event, but as seen using the IVT direction (vectors) and intensity (kg m^{-1} s^{-1}; color shading) at 0000 UTC 26 May 2013 obtained from ERAI; and (bottom) as in the middle panel, but for NCEP-2 data. The reference meridian at 15°E (in red) used in the identification method is also shown in the middle and bottom panels.

ERAI (NCEP-2). This was calculated using the 1200 UTC data for each day from 1979 to 2014. For ERAI, the threshold value was 327 kg m^{-1} s^{-1}, while for NCEP-2, it was 321 kg m^{-1} s^{-1}.

2) For each 6-hourly time step in the reanalysis, the maximum value in IVT was determined for the grid points between 27.75°and 35.25°S (27.5°–35.0°S), along the 15°E reference meridian in ERAI (NCEP-2). If the value exceeded the threshold in the previous step, the grid point was flagged.
3) A backward/forward search was performed to identify the maximum IVT at each longitude, with the location of the grid points that exceeded the IVT threshold (derived in step 1) being tracked.
4) The final step was to determine if the values exceeding the threshold extended over many

degrees longitude in order to classify it as an AR. Taking into account that the length of a degree at 35°S is approximately ±90 km and the resolution of the reanalysis data, it was determined that 27 contiguous points ($27 \times 0.75° = 20.25° = \pm1823$ km) in ERAI and 8 in NCEP-2 ($8 \times 2.5° = 20 = \pm1800$ km) exceeding the threshold would satisfy the length criteria of an AR. This condition was checked every 6 h, with it being considered an AR time step when it was fulfilled.

From the output above, ARs were further classified as being either persistent or nonpersistent, with the former simply referring to ARs that contained at least three uninterrupted time steps or 18 h of persistence (Lavers et al. 2012; Lavers and Villarini 2013; Ramos et al. 2015). A persistent AR was counted as distinct from another persistent AR if it was separated by more than a day or four time steps. Only persistent ARs are included in the climatological aspects of the analysis here, while nonpersistent ARs are included in the extreme event analysis.

c. *Attribution of winter rainfall and daily extreme events to ARs*

Daily rainfall data over South Africa were provided by the South African Weather Service (SAWS) for the period from May 1979 to September 2014. Although there are numerous stations (~500) across the region, with some extending back as early as 1850 and containing data through the end of 2015, not all have a full record of data. Thus, only stations that passed quality control tests (after Durre et al. 2010) and those with less than 5% missing data (i.e., 95% valid data available) during the main winter months (May–September) for the period 1979–2014 are used (note that the month of April is excluded here for lack of data availability). Furthermore, only stations that fell within the two local key river basins in the southwestern part of the country were considered. As a result, only 45 stations were retained for the analysis (see Fig. 1 for locations). The contribution of ARs to the winter rainfall was determined by adding up the rainfall at each station on the day and the day following the occurrence of a persistent AR being identified off the west coast of South Africa. A similar approach has been used along the west coast of North America (e.g., Rutz and Steenburgh 2012). The contribution to monthly and winter totals is then calculated based on the daily data associated with the ARs.

The ranking of daily extremes is based on a method that has been adapted from Ramos et al. (2014). It is used to characterize and rank each winter day, taking into account the severity of the rainfall anomaly and its spatial extent. However, instead of being based on the normalized departure for each day at each station, as in the original method, the 95th-percentile threshold value is used for each Julian day. The primary reason for using this percentile-based method instead of the normalization procedure applied by Ramos et al. (2014) is that the latter does not ensure a typical Gaussian distribution at each station. Therefore, for each station and each Julian day, the 95th-percentile value was determined, taken over the reference period 1979–2014. Only days with rainfall exceeding 1 mm were taken into account. A 7-day running mean was then applied to smooth the 95th-percentile threshold climatological time series. Ramos et al. (2014) note that the length of the smoothing filter (e.g., 7 vs 21 days) does not significantly alter the ranking of the days. An anomaly value was then calculated by subtracting the rainfall of each day from this daily climatological 95th-percentile threshold. A new value R was computed, which is the magnitude/extent of the event and is obtained by

1) determining the percentage of stations that contained a positive anomaly value on each given day (hereafter N and in %);
2) the mean value of anomalies across the stations that contained a positive value (hereafter M and in mm); and
3) the extent and magnitude of the extreme R is determined by multiplying $N \times M$ (the higher the R value, the more extreme the daily event). The highest value of R then corresponds to the first day in the extreme ranking.

This method was applied to all the stations within the domain over the southwestern part of South Africa. It should be noted that this method does not take into account if actual flooding occurred with the extreme rainfall day identified. This is because other factors, such as antecedent rainfall or topography of the basin, are not considered here.

3. South Atlantic AR climatology

Over the 36-yr period in ERAI data, a total of 367 persistent ARs were identified as crossing 15°E between 27.75° and 35.25°S during the winter months, which corresponds to a mean of 10.2 events per winter (standard deviation of 3.14). In comparison, in NCEP-2 data over the same period, a total of 526 persistent ARs were identified, with an average of 14.6 per winter (standard deviation of 3.92). The difference between these two reanalysis products could be predominantly ascribed to 1) the different IVT threshold values used for each reanalysis, 2) the different native grid resolutions, or 3) the different assimilation methods used by the different

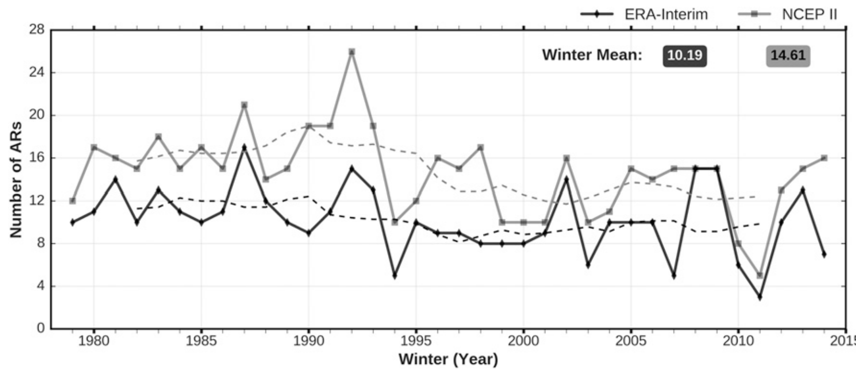

FIG. 3. Interannual variability in the number of persistent ARs identified off the west coast of South Africa during the winter months (April–September) for 1979–2014 in ERAI (black line) and NCEP-2 (light gray line). The winter mean for each reanalysis is given in the top-right corner. The black and gray dashed lines are the 7-yr running means for ERAI and NCEP-2, respectively.

models to create the reanalyses (Lavers et al. 2012; Ramos et al. 2015). These values are comparable to those identified in the North Atlantic, making landfall in Great Britain (Lavers et al. 2012) or over the Iberian Peninsula (Ramos et al. 2015). In the North Pacific, Neiman et al. (2008) document that in California, an average of 15 events per year are recorded; however, this is based on all seasons, a shorter study period (1998–2005), and using SSM/I data. Apart from the total number of ARs found in each reanalysis, there is relatively good agreement in terms of interannual variability between the two datasets (Fig. 3). The Pearson correlation coefficient between the two is 0.67 (p value < 0.005). The minimum number of AR events recorded for a winter season is 3 (5), while the maximum is 17 (26) in the ERAI (NCEP-2) data (not necessarily the same year).

AR activity tends to peak early in the winter season (May) and slowly decreases throughout the winter (Fig. 4). This cycle is more distinct in the ERAI data compared to NCEP-2, with the latter showing similar AR activity in June and July to that in May. The early winter peak found here is marginally earlier than that found in ARs in the North Atlantic, which tend to peak in activity during December (Ramos et al. 2015). The month of May also has the largest range in AR activity in the South Atlantic (0–7 events) in ERAI, whereas in NCEP-2, June is found to have the largest range (0–8 events).

Just over half (~54%) of the persistent ARs identified in NCEP-2 in the South Atlantic tend to have a duration of fewer than 30 h (Fig. 5a), with a similar percentage found in ERAI (~55%). Around 30% of the ARs persist longer than 1.5 days (36 h) in NCEP-2, with a similar percentage found in ERAI. Overall, the average duration (from first to last time step in identification) of these features is just over 30 h in both NCEP-2 and ERAI. The range of these duration statistics falls within that documented elsewhere, such as ARs penetrating the Iberian Peninsula (Ramos et al. 2015) and California (Ralph et al. 2013). It is worth noting that there were 352 (536) cases in the ERAI (NCEP-2) reanalysis in which an AR was identified as satisfying the IVT and length thresholds, but failed in terms of persistence (i.e., had fewer than three time steps) and was therefore not included in this section for analysis.

In terms of maximum IVT values during the life cycle of persistent ARs, around 75% of the systems contain a maximum IVT of between 400 and 650 $kg\,m^{-1}\,s^{-1}$ in NCEP-2, while in ERAI, only around 60% are binned in that range (Fig. 5b). Conversely, a higher percentage of systems in the ERAI data have a maximum IVT exceeding 650 $kg\,m^{-1}\,s^{-1}$ than those found in NCEP-2. A very similar spread in IVT is found at the initial maximum as the system passes 15°E (not shown). At the initial identification stage of the ARs along 15°E, the maximum IVT value in the majority of the events is located in the southernmost grid point at 35.25°S in ERAI (not shown). This spatial pattern is also found in the maximum IVT during the entire life cycle of an AR in ERAI, with ~65% of the events having a maximum IVT at the southernmost grid point (Fig. 5c). The lower-resolution NCEP-2 reanalysis reveals that an almost equal number of ARs occur at the grid points located at 32.5°S as compared with 35°S (not shown). The analysis also reveals that very few persistent ARs were identified equatorward of 30°S in both reanalysis datasets, with only 11 ARs in ERAI and 19 in NCEP-2 over the full period (not shown). Given the close links between ARs and extratropical disturbances (e.g., Cordeira et al. 2013;

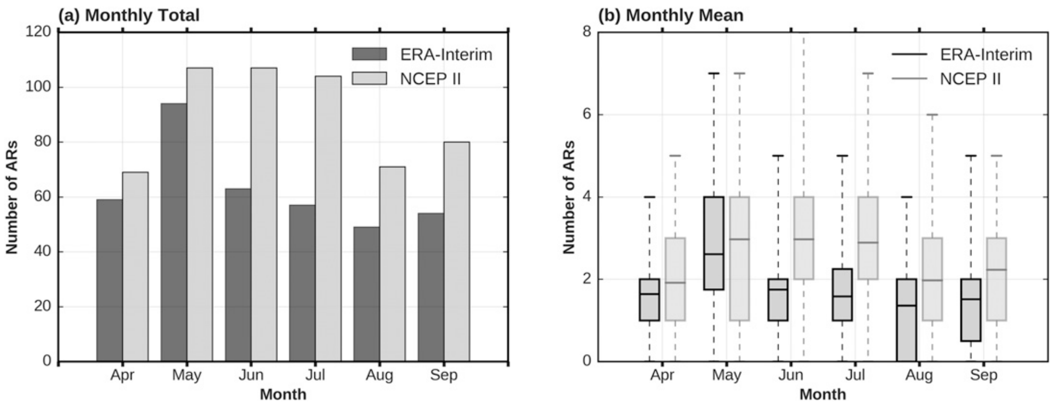

FIG. 4. (a) Intra-annual variability of the number of persistent ARs off the west coast of South Africa in the ERAI (dark gray bars) and NCEP-2 (light gray bars) reanalyses. (b) Box plots illustrating the monthly mean and range in AR activity in ERAI (dark gray box) and NCEP-2 (light gray box) reanalyses for the period 1979–2014. The horizontal line in each box is the mean, while the vertical lines indicate the minimum and maximum number of ARs.

Dacre et al. 2015; Ramos et al. 2015), it is likely that this AR spatial pattern is linked to the extratropical cyclone activity to the south of the country, with generally few cold fronts impacting at lower latitudes on the west coast (29°–34.5°S) compared with the southern part of the domain (e.g., Jones and Simmonds 1993; Hoskins and Hodges 2005). Furthermore, the location of the South Atlantic subtropical high (SASH) could also play a key role in fewer ARs impacting at lower latitudes on the west coast. During the early autumn months, the center of SASH is typically located around 27°–28°S, but it shifts equatorward during May and is positioned around 24°–25°S during the winter months (Sun et al. 2017). Not only would this impact the location of ARs making landfall along the west coast, but it would also play a role on the overall seasonal cycle of ARs described earlier.

Figure 5c also highlights the influence that the location of the domain can have on the statistics of the AR climatology presented here. Although there is some consistency in the data and methods adopted to build this AR climatology, an additional factor to consider when comparing ARs in the different ocean basins is the domain used. As an example, Lavers et al. (2012) concentrate on ARs that transect 4°W in grid points between 50° and 60°N, and Ramos et al. (2015) focus on grid points centered along 10°W between 35° and 45°N, whereas a slightly smaller domain (27.5°–35.25°S) is used here. Therefore, considering the maximum location of AR activity presented here is at the southernmost latitude of the domain (35.25°S; Fig. 5c), it is likely that the frequency (underestimation) and location of ARs in the South Atlantic are not completely represented. However, the main focus of this study is the contribution of ARs to total rainfall and in extreme rainfall events in South Africa, as discussed in the following section.

4. AR contribution to winter rainfall

a. *Winter rainfall totals*

Rainfall in the southwest region of South Africa is known to contain considerable interannual variability (Fig. 6). The correlation coefficient between anomalous AR activity and that of the standardized anomaly in winter rainfall is 0.43 (p value = 0.008) in ERAI and 0.46 (p value = 0.005) in NCEP-2. When broken down to individual stations, a stronger relationship is evident. The maximum correlation between anomalous AR activity and standardized winter rainfall at an individual station reaches 0.52 (0.56) in ERAI (NCEP-2), both with p values < 0.05 (Fig. 7). In most cases, the stations with the strongest relationship with AR activity are located in the mountainous regions, which include the stations immediately surrounding Cape Town (Fig. 1 vs Fig. 7). The weakest correlation between station rainfall and AR activity is at stations located farther up the drier west coast or to the far east of the domain, where the moisture has been largely depleted after undergoing the foehn effect of the coastal mountains.

The relatively weak link between AR activity and stations located in the eastern part of the domain is evident when one breaks down the average contribution of ARs to total winter season rainfall (Fig. 8). The stations in the east contain the lowest contribution in both reanalysis datasets (15%–25% in ERAI and 25%–40% in NCEP-2). The low contributions located at stations farthest east could imply that most of the water vapor is

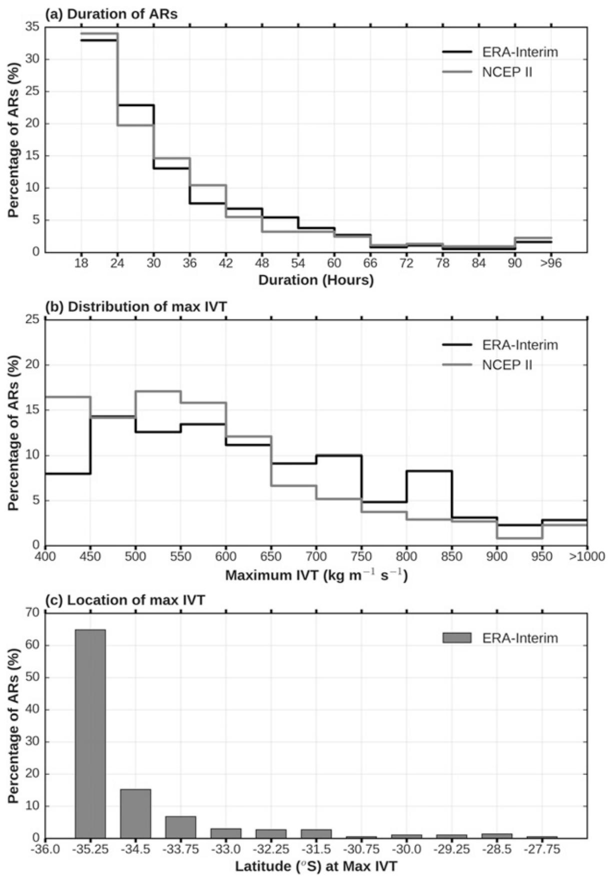

FIG. 5. (a) Distribution (%) of the duration (binned at 6-h intervals) of the persistent AR events in the 6-hourly reanalysis data, with black lines representing ERAI and gray lines representing NCEP-2. (b) As in (a), but for maximum IVT for each persistent AR (binned at 50 kg m^{-1} s^{-1} intervals). (c) The latitude (27.75°–35.25°S) at which the maximum IVT occurred in ERAI data only.

lost through rainfall as the AR passes over the mountains to the west of these stations. A similar rain shadow process is argued as being one of the main factors that determines rainfall contributions by ARs in the western United States (Rutz et al. 2014).

The highest contributions in the southwest region of South Africa during the winter season are typically found at stations located in the mountain regions positioned immediately to the east of Cape Town, which are directly impacted by rain-bearing westerly winds in this season. Average AR contributions at these stations typically exceed 40% (50%) of the total winter rainfall in ERAI (NCEP-2); that is to say, depending on the reanalysis data used, over half the winter rainfall at some stations occurred on the day or the day after an AR made landfall along the west coast. It is worth noting that the overall higher percentage in NCEP-2 is likely due to the higher number of ARs identified using that particular dataset (Fig. 3).

The influence that AR activity can have on rainfall at the various stations is also evident on the monthly time scale (Fig. 9). The highest average contribution is typically found during the early winter months (May and June), when AR activity is most frequent (Fig. 4). In May, more than half the rainfall at many stations occurred on the day or the day after an AR made landfall along the west coast (Fig. 9a). The lowest contribution, on average, occurs in August (Fig. 9d), the month when the fewest ARs occur off the west coast (Fig. 4). There is again a difference in AR contribution to winter rainfall between the two reanalysis products, which is likely because of the number of ARs identified in both. Results from NCEP-2 (not shown) suggest that ARs have a greater influence on local rainfall, particularly during May–July. Over 45% of the rainfall at many stations located in the western part of the domain can be linked to AR activity during the early winter months. ARs tend to have less of an impact during the late winter months, similar to that in the ERAI reanalysis. There is also a very similar spatial pattern between the two reanalyses, with stations located in the east having a much lower AR-related rainfall contribution than that found in the stations in the western part of the domain.

b. ARs and extreme events

The top nine extreme daily rainfall events determined for the southwestern part of South Africa are presented in Fig. 10. Of these nine events, eight are in some way associated with an AR. This was determined by matching the days on which ARs were identified (both persistent and nonpersistent) in the reanalysis to those of the ranked extreme rainfall days found in the station data, an approach similar to that undertaken for the Iberian Peninsula (Ramos et al. 2015). It should be noted that the only extreme event ranked in the top nine that is not linked with an AR is the fifth event on 7 August 2013. For this event, most of the heavy rainfall took place in the southeastern part of the domain or the leeward side of the coastal mountains, which, as described in the previous section, typically has the lowest association with AR activity in the region (e.g., Fig. 8).

The eight extreme events can be further classified: four of them (six in NCEP-2) are linked to a persistent AR in both reanalyses, while the remaining three (one in NCEP-2) contain no more than two time steps linked with ARs (i.e., nonpersistent). There is some disagreement between the two reanalysis products, with events ranked 1 and 8 having an AR identified in only one of the reanalysis datasets, whereas the rest have an AR in both products. As described in section 3, each reanalysis product does not necessarily capture the same AR event. This could be partly due to the different IVT

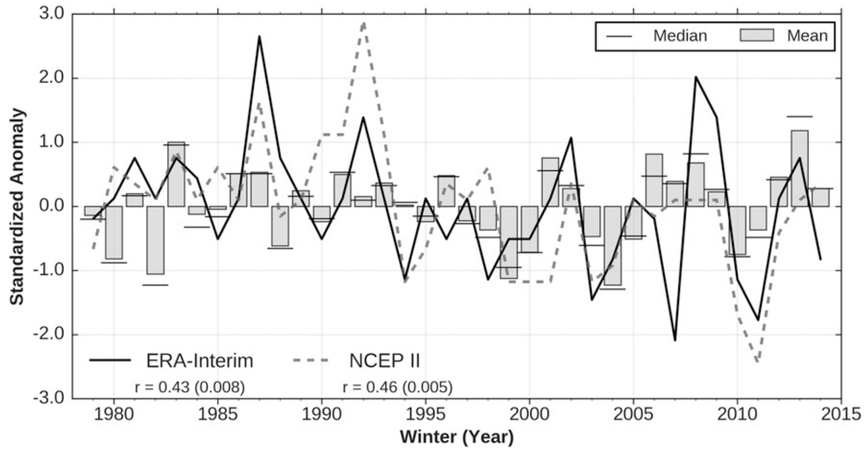

FIG. 6. Standardized anomaly of winter rainfall (May–September) across the weather stations within the domain for the period 1979–2014. The gray bars are the mean anomaly across the stations, while the thin black horizontal line denotes the median anomaly. The solid black and dashed gray lines are the standardized anomaly of winter ARs (only May–September) in ERAI and NCEP-2, respectively. The Pearson correlation coefficient (p value) between the rainfall and AR activity is highlighted in the bottom-left corner.

threshold used, or the different grid resolutions, which as noted by Lavers et al. (2012), could account for locating ARs in slightly different areas.

Further analysis of the top 50 ranked events shows that 26 (36) extreme rainfall events can be linked to persistent ARs (when including nonpersistent ARs) in the ERAI data. In NCEP-2, the result is slightly different, with 31 (34) of the top 50 extreme rainfall events being linked to persistent (including nonpersistent) ARs. Thus, although persistent ARs are not necessarily a prerequisite for extreme daily rainfall in the region, the majority of the top daily extreme events linked to ARs are associated with persistent ones. Overall, these results regarding the contribution of ARs to extreme rainfall events in the southwestern region of South Africa are very similar to those documented elsewhere, such as the Iberian Peninsula (Ramos et al. 2015). However, when looking for clear fingerprints of AR characteristics or features that could be indicative of extreme rainfall potential, no clear pattern emerges. The ARs associated with the top 50 extreme daily rainfall events identified here contain insufficient common characteristics in terms of duration, mean or maximum IVT, or preferred latitude for straightforward classification purposes. This may hamper the forecasting potential in the short term, although further research may provide new insights on these links between certain ARs and top rainfall events. For example, Hecht and Cordeira (2017) have recently shown that certain features of ARs, such as orientation or intensity, can have a large influence on the precipitation patterns in the California Russian River watershed. Increased commonality for the South African domain could perhaps be obtained by using higher-resolution input data or through an increase in the number of AR-associated extreme rainfall cases once a longer record becomes available.

5. Discussion and conclusions

Based on the methodology developed by Lavers et al. (2012) and Lavers and Villarini (2013), a climatology of persistent ARs impinging on the west coast of South Africa during the austral winter months (April–September) was developed for the period 1979–2014. Input data for the identification are based on two reanalysis products, namely, the relatively high-resolution ERAI and the lower-resolution NCEP-2. The findings suggest that although ARs occur throughout the winter months, they occur more frequently during the month of May (May–July) in ERAI (NCEP-2). On average, 10–15 ARs occur through the winter period, but this number varies significantly from year to year, as it can be as low as 3 or as high as 26. However, the AR climatological statistics are influenced by the input data, with the number of ARs in ERAI being around 30% less overall than that in NCEP-2. The lower number of ARs identified in the higher-resolution ERAI was also noted by Ramos et al. (2015) for ARs in the North Atlantic. The influence the choice of reanalysis can have on AR identification has previously been documented by Lavers et al. (2012).

Compared to their Northern Hemisphere counterparts, ARs in the South Atlantic do not make landfall as

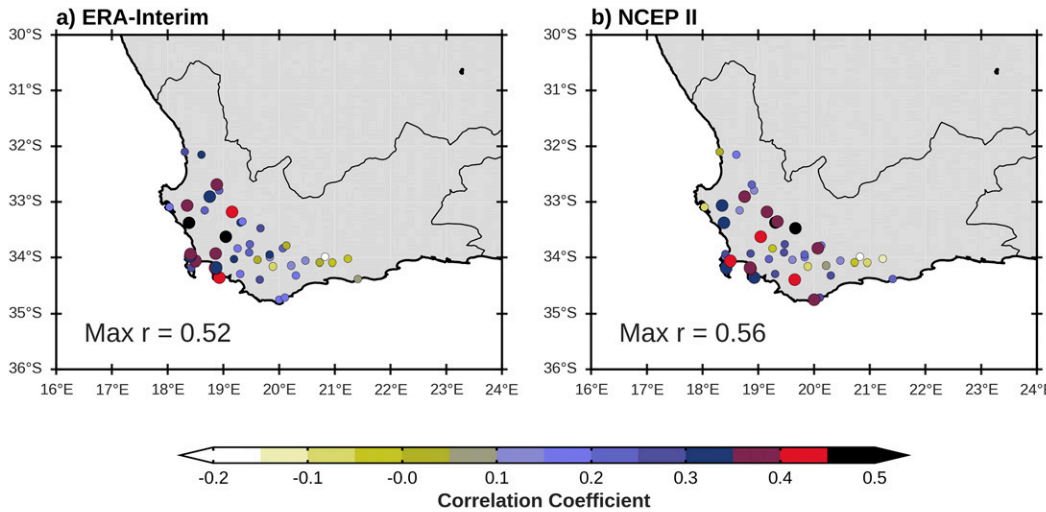

FIG. 7. Pearson correlation coefficient for the standardized anomaly of ARs per winter for the period 1979–2014 (see Fig. 6) in (a) ERAI and (b) NCEP-2, and the standardized anomaly of the total winter rainfall at each station. Stations with a p value < 0.05 are represented by larger circles. The maximum correlation among all the stations is given in the bottom-left corner.

frequently. This is not to say that fewer AR events occur in the South Atlantic, but is rather related to the latitudinal extent of the continents. In many cases, the plume of moisture passes to the south of the African continent, which terminates at 34°–35°S (somewhat lower latitude than the Iberian Peninsula or the Russian River region in California). This is supported by the maximum AR activity occurring at the grid point located most poleward in the predefined domain used here, which was restricted to the west coast of South Africa. Thus, it is likely that if the choice domain was extended farther poleward, more ARs would be accounted for in the South Atlantic than in the domain presented here.

The findings here regarding the role ARs can play in the overall contribution to seasonal totals or to extreme rainfall events are comparable to those documented elsewhere (e.g., Ralph et al. 2006; Dettinger et al. 2011; Rutz and Steenburgh 2012; Lavers and Villarini 2015; Ramos et al. 2015). Although there is some local

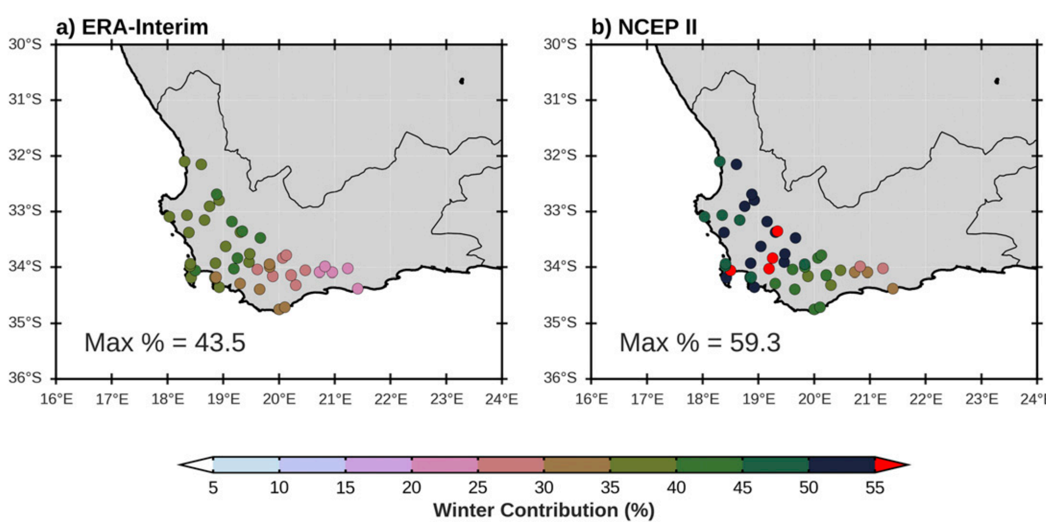

FIG. 8. Mean percentage of the total winter (May–September) precipitation at the SAWS weather stations occurring on the day or day after a persistent AR is located off the west coast of South Africa in (a) ERAI and (b) NCEP-2, over the period 1979–2014. The maximum contribution (%) is given in the bottom left corner of the panel.

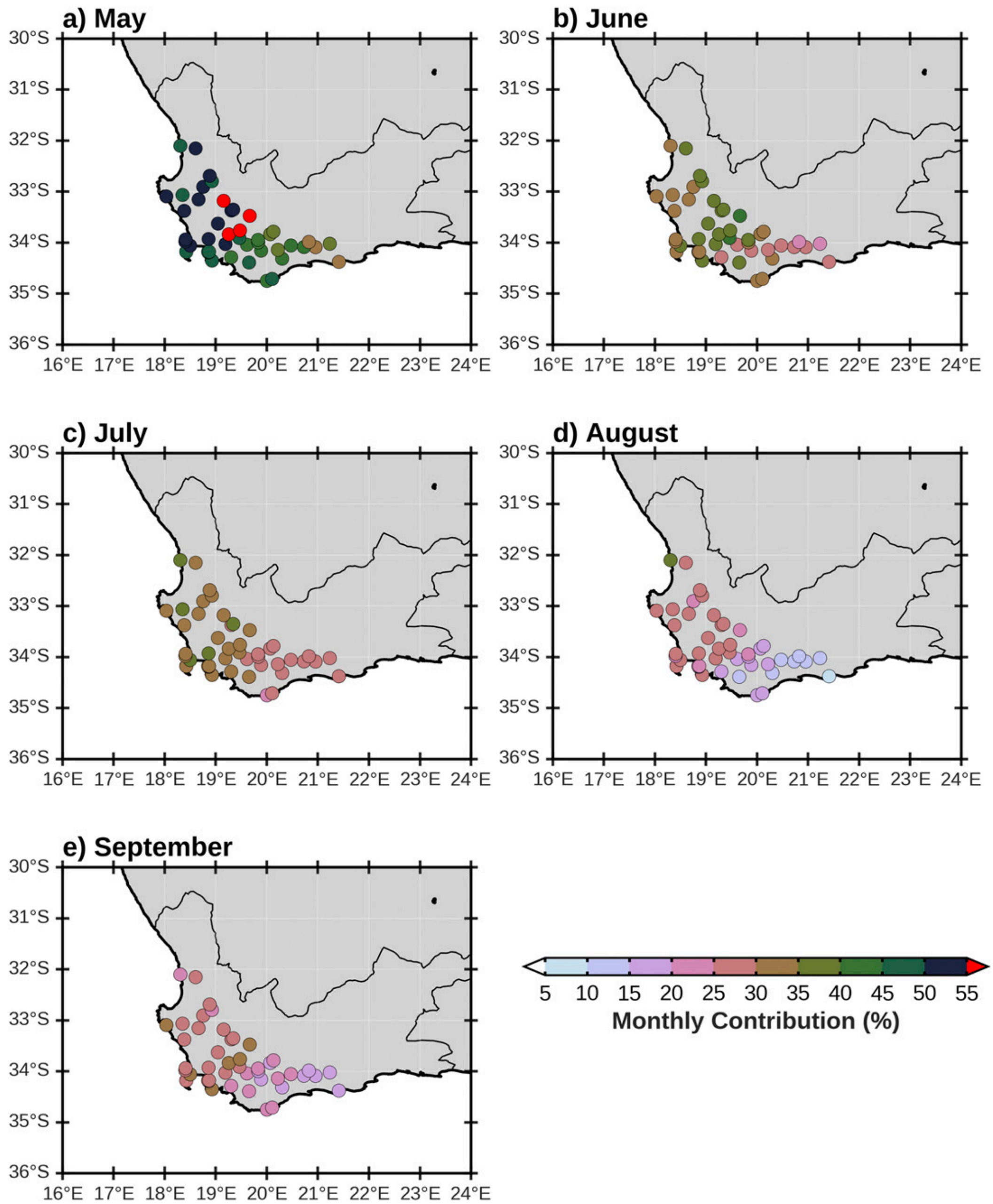

FIG. 9. Mean percentage of the total monthly precipitation at the SAWS weather stations occurring on the day or day after a persistent AR is located off the west coast of South Africa in the ERAI data (1979–2014) only. The month is given at the top-left corner of each panel.

variability regarding the influence of ARs on rainfall at the stations, there are some obvious patterns. Depending on the reanalysis product, ARs were found to contribute between 15% and 60% of the total winter rainfall at stations across the southwestern region of South Africa. The highest winter season contributions are typically found at stations located in the mountain regions immediately to the east of Cape Town, closer to the South Atlantic coast. The lowest contributions are located at stations farthest east, which suggests that most of the water vapor is lost through rainfall as the AR passes over the mountains to the west of these stations, so these stations are in a relative rain shadow. The highest average monthly contributions occur during the early winter months (May and June), when ARs are most frequent.

In terms of extreme rainfall, around 70% of the top 50 daily winter rainfall extremes in southwestern South

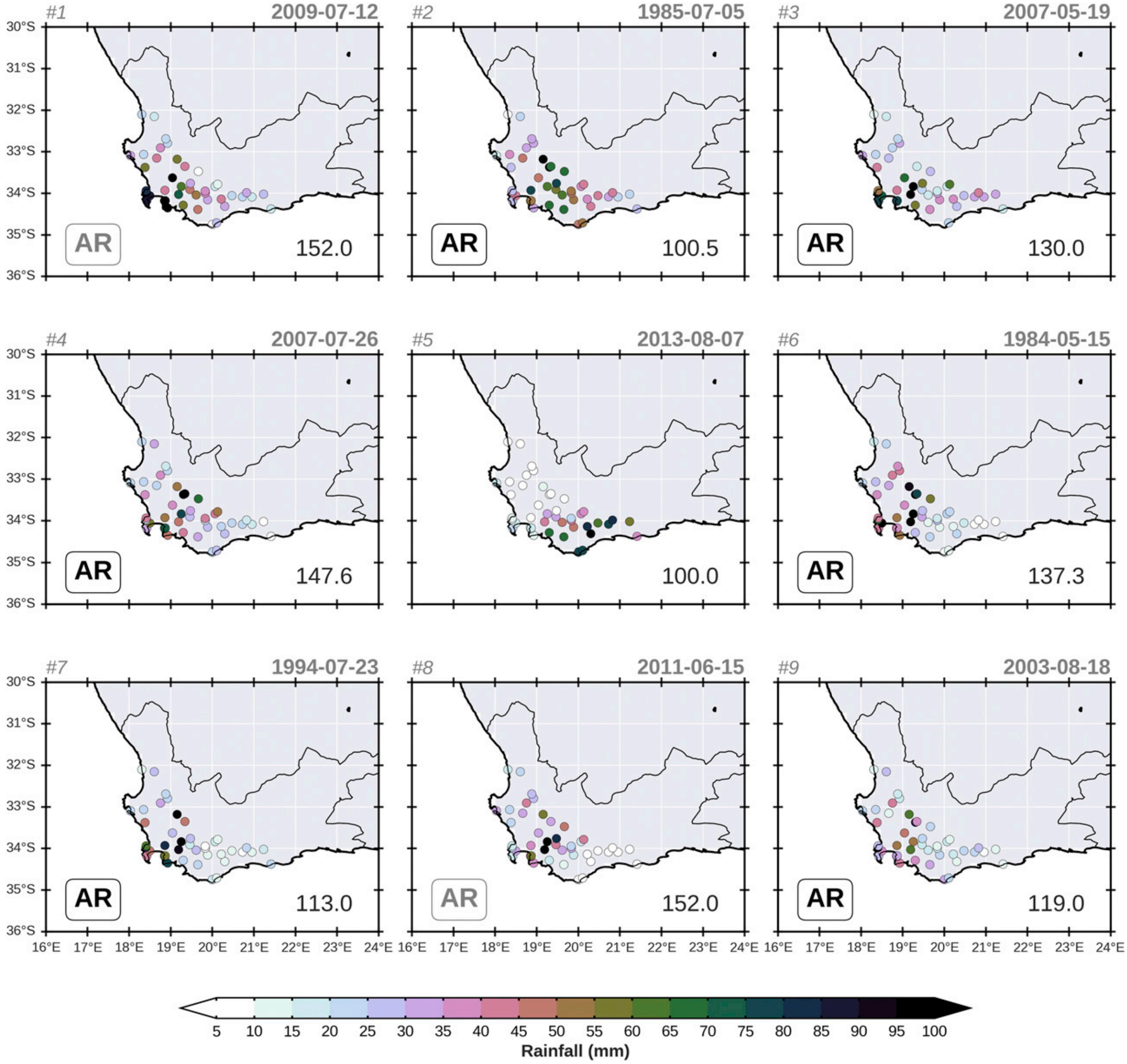

FIG. 10. The top nine extreme precipitation days for the southwestern tip of South Africa. The rank and day of the event are given in the top-left and top-right corners of each panel, respectively. The maximum amount of precipitation for that particular day is given in the bottom-right corner of each panel (mm). Events that are linked to an AR (including nonpersistent ARs) are denoted by the letters ''AR'' in the bottom-left corner; letters in gray signify the event is linked to an AR being identified in only one of the reanalysis products.

Africa were linked in some way to ARs. If only persistent ARs were taken into consideration, this value drops to just over 50% (closer to 60% in NCEP-2). This suggests that although persistent ARs are important contributors to heavy rainfall events, they are not necessarily a prerequisite. Other features of the ARs, such as the direction of the IVT transport, are known to play an important role in local rainfall characteristics over California (e.g., Hecht and Cordeira 2017), and the same could apply here. It should also be noted that these daily rainfall extremes are not necessarily associated with local flooding because the methodology used does not take into account other important factors, such as antecedent rainfall (soil saturation), geological setting, catchment size, land use, and management of local rivers/dams. Nevertheless, it still provides some insight into the possibility for improved local flood forecasting, particularly in the mountainous region, based on the development and identification of a persistent AR off the west coast of South Africa.

Overall, these results improve our understanding of the importance of ARs for regional rainfall patterns along the west coast of South Africa. The next scientific challenge is to investigate and understand factors that influence the formation and location of ARs in the South Atlantic. This includes investigating the influence of South American climate variability on African climate, which has not been well documented. Grimm and Reason (2015) investigated the link between climate variability in the South America monsoon region and summer and winter rainfall patterns over southern Africa. During the winter months, these authors note a 4–5-day lag in the positive correlation between rainfall in southeastern South America and in southwestern South Africa. Their findings suggest that the link between the two regions may occur directly via atmospheric circulation anomalies induced by convection over South America. Another potential link between the two regions during the winter months could be through water vapor transport via ARs, with South America acting as a moisture source. Furthermore, it is understood that the southwest Atlantic Ocean is a region of intense cyclogenesis (Bengtsson et al. 2006; Hoskins and Hodges 2005). Considering the close association between ARs and midlatitude cyclones, it is likely that regional climate dynamics off the east coast of South America could play a key role in winter rainfall in South Africa. Thus, the potential links between moisture availability in South America, the formation and location of midlatitude cyclones, and winter rainfall in South Africa warrant further investigation.

Finally, midlatitude atmospheric water vapor content is expected to rise in a warmer climate due to an increase in saturation water vapor pressure with air temperature, as governed by the Clausius–Clapeyron equation (Held and Soden 2006). This has the potential to result in increased water vapor transport through ARs (Gimeno et al. 2016). The link between increased AR activity/intensity through climate change and local flooding has already been projected for some regions, such as California (Dettinger 2011), Great Britain (Lavers et al. 2013), and western Europe (Ramos et al. 2016). Given the results highlighting the impact ARs have on heavy regional winter rainfall events, this implies, all else being equal, that there may be an increased risk of flooding events in the southwest region of South Africa in the future through changes in AR activity. This again highlights the need to better understand the factors that influence the formation, frequency, and intensity of ARs in the South Atlantic. Given the close association between these ARs and the winter rainfall region of South Africa, this could potentially play a key role in understanding any local changes in the context of global climate change.

Acknowledgments. The NCEP-2 data were provided by NOAA/OAR/ESRL PSD (Boulder, CO; http://www.esrl.noaa.gov/psd/), and the ERAI data were obtained from the Meteorological Archival and Retrieval System (MARS) at the ECMWF. We thank the South African Weather Service for providing the station data and Pierre Kloppers for the data management. We would also like to thank the reviewers for their insightful comments that helped improve the manuscript. Ross Blamey and Chris Reason were supported by the Natural Environment Research Council (NERC) Future Climate for Africa (FCFA) regional consortium project UMFULA (NE/M020223/1). Alexandre Ramos, Ricardo Trigo, and Chris Reason were supported by the project Improving Drought and Flood Early Warning, Forecasting and Mitigation using real-time hydroclimatic indicators (IMDROFLOOD) funded by Fundação para a Ciência e a Tecnologia, Portugal (FCT) (WaterJPI/0004/2014) and the Water Research Commission (K5-2618). Alexandre M. Ramos was also supported by an FCT postdoctoral grant (FCT/DFRH/SFRH/BPD/84328/2012).

REFERENCES

Bao, J.-W., S. A. Michelson, P. J. Neiman, F. M. Ralph, and J. M. Wilczak, 2006: Interpretation of enhanced integrated water vapor bands associated with extratropical cyclones: Their formation and connection to tropical moisture. *Mon. Wea. Rev.*, **134**, 1063–1080, https://doi.org/10.1175/MWR3123.1.

Bengtsson, L., K. I. Hodges, and E. Roeckner, 2006: Storm tracks and climate change. *J. Climate*, **19**, 3518–3543, https://doi.org/10.1175/JCLI3815.1.

Blamey, R., and C. J. C. Reason, 2007: Relationships between Antarctic sea-ice and South African winter rainfall. *Climate Res.*, **33**, 183–193, https://doi.org/10.3354/cr033183.

Cordeira, J. M., F. M. Ralph, and B. J. Moore, 2013: The development and evolution of two atmospheric rivers in proximity to western North Pacific tropical cyclones in October 2010. *Mon. Wea. Rev.*, **141**, 4234–4255, https://doi.org/10.1175/MWR-D-13-00019.1.

Dacre, H. F., P. A. Clark, O. Martinez-Alvarado, M. A. Stringer, and D. A. Lavers, 2015: How do atmospheric rivers form? *Bull. Amer. Meteor. Soc.*, **96**, 1243–1255, https://doi.org/10.1175/BAMS-D-14-00031.1.

Dee, D. P., and Coauthors, 2011: The ERA-Interim reanalysis: Configuration and performance of the data assimilation system. *Quart. J. Roy. Meteor. Soc.*, **137**, 553–597, https://doi.org/10.1002/qj.828.

Dettinger, M., 2011: Climate change, atmospheric rivers, and floods in California—A multimodel analysis of storm frequency and magnitude changes. *J. Amer. Water Resour. Assoc.*, **47**, 514–523, https://doi.org/10.1111/j.1752-1688.2011.00546.x.

——, F. M. Ralph, T. Das, P. J. Neiman, and D. R. Cayan, 2011: Atmospheric rivers, floods and the water resources of California. *Water*, **3**, 445–478, https://doi.org/10.3390/w3020445.

Durre, I., M. J. Menne, B. E. Gleason, T. G. Houston, and R. S. Vose, 2010: Comprehensive automated quality assurance of daily surface observations. *J. Appl. Meteor. Climatol.*, **49**, 1615–1633, https://doi.org/10.1175/2010JAMC2375.1.

Gimeno, L., R. Nieto, M. Vázquez, and D. A. Lavers, 2014: Atmospheric rivers: A mini-review. *Front. Earth Sci.*, **2**, 2, https://doi.org/10.3389/feart.2014.00002.

——, and Coauthors, 2016: Major mechanisms of atmospheric moisture transport and their role in extreme precipitation events. *Annu. Rev. Environ. Resour.*, **41**, 117–141, https://doi.org/10.1146/annurev-environ-110615-085558.

Grimm, A. M., and C. J. C. Reason, 2015: Intraseasonal teleconnections between South America and South Africa. *J. Climate*, **28**, 9489–9497, https://doi.org/10.1175/JCLI-D-15-0116.1.

Hecht, C. W., and J. M. Cordeira, 2017: Characterizing the influence of atmospheric river orientation and intensity on precipitation distributions over north coastal California. *Geophys. Res. Lett.*, **44**, 9048–9058, https://doi.org/10.1002/2017GL074179.

Held, I. M., and B. J. Soden, 2006: Robust responses of the hydrological cycle to global warming. *J. Climate*, **19**, 5686–5699, https://doi.org/10.1175/JCLI3990.1.

Hirota, N., Y. N. Takayabu, M. Kato, and S. Arakane, 2016: Roles of an atmospheric river and a cutoff low in the extreme precipitation event in Hiroshima on 19 August 2014. *Mon. Wea. Rev.*, **144**, 1145–1160, https://doi.org/10.1175/MWR-D-15-0299.1.

Hoskins, B. J., and K. I. Hodges, 2005: A new perspective on Southern Hemisphere storm tracks. *J. Climate*, **18**, 4108–4129, https://doi.org/10.1175/JCLI3570.1.

Jones, D. A., and I. Simmonds, 1993: A climatology of Southern Hemisphere extratropical cyclones. *Climate Dyn.*, **9**, 131–145, https://doi.org/10.1007/BF00209750.

Junker, N. W., R. H. Grumm, R. Hart, L. F. Bosart, K. M. Bell, and F. J. Pereira, 2008: Use of normalized anomaly fields to anticipate extreme rainfall in the mountains of Northern California. *Wea. Forecasting*, **23**, 336–356, https://doi.org/10.1175/2007WAF2007013.1.

Kalnay, E., and Coauthors, 1996: The NCEP/NCAR 40-Year Reanalysis Project. *Bull. Amer. Meteor. Soc.*, **77**, 437–471, https://doi.org/10.1175/1520-0477(1996)077<0437:TNYRP>2.0.CO;2.

Kanamitsu, M., W. Ebisuzaki, J. Woollen, S. K. Yang, J. Hnilo, M. Fiorino, and G. L. Potter, 2002: NCEP–DOE AMIP-II Reanalysis (R-2). *Bull. Amer. Meteor. Soc.*, **83**, 1631–1643, https://doi.org/10.1175/BAMS-83-11-1631.

Lavers, D. A., and G. Villarini, 2013: The nexus between atmospheric rivers and extreme precipitation across Europe. *Geophys. Res. Lett.*, **40**, 3259–3264, https://doi.org/10.1002/grl.50636.

——, and ——, 2015: The contribution of atmospheric rivers to precipitation in Europe and the United States. *J. Hydrol.*, **522**, 382–390, https://doi.org/10.1016/j.jhydrol.2014.12.010.

——, R. P. Allan, E. F. Wood, G. Villarini, D. J. Brayshaw, and A. J. Wade, 2011: Winter floods in Britain are connected to atmospheric rivers. *Geophys. Res. Lett.*, **38**, L23803, https://doi.org/10.1029/2011GL049783.

——, G. Villarini, R. P. Allan, E. F. Wood, and A. J. Wade, 2012: The detection of atmospheric rivers in atmospheric reanalyses and their links to British winter floods and the large-scale climatic circulation. *J. Geophys. Res.*, **117**, D20106, https://doi.org/10.1029/2012JD018027.

——, R. P. Allan, G. Villarini, B. Lloyd-Hughes, D. J. Brayshaw, and A. J. Wade, 2013: Future changes in atmospheric rivers and their implications for winter flooding in Britain. *Environ. Res. Lett.*, **8**, 034010, https://doi.org/10.1088/1748-9326/8/3/034010.

Liniger, H., R. Weingartner, and M. Grosejean, 1998: Mountains of the world: Water towers for the 21st century. University of Bern Centre for Development and Environment Tech. Rep., 32 pp.

Messerli, B., D. Viviroli, and R. Weingartner, 2004: Mountains of the world: Vulnerable water towers for the 21st century. *Ambio Spec. Rep.*, **13**, 29–34.

Midgley, G. F., and Coauthors, 2007: Assessing impacts, vulnerability and adaptation in key South African sectors: An input into the Long Term Mitigation Scenarios process. University of Cape Town Energy Research Centre Rep., 24 pp., http://www.erc.uct.ac.za/sites/default/files/image_tool/images/119/Papers-2007/07Midgley-etal-LTMS_Impacts_Vulnerability_Adaptation.pdf.

Moore, B. J., P. J. Neiman, F. M. Ralph, and F. E. Barthold, 2012: Physical processes associated with heavy flooding rainfall in Nashville, Tennessee, and vicinity during 1–2 May 2010: The role of an atmospheric river and mesoscale convective systems. *Mon. Wea. Rev.*, **140**, 358–378, https://doi.org/10.1175/MWR-D-11-00126.1.

Neiman, P. J., F. M. Ralph, A. B. White, D. E. Kingsmill, and P. O. G. Persson, 2002: The statistical relationship between upslope flow and rainfall in California's coastal mountains: Observations during CALJET. *Mon. Wea. Rev.*, **130**, 1468–1492, https://doi.org/10.1175/1520-0493(2002)130<1468:TSRBUF>2.0.CO;2.

——, ——, G. A. Wick, J. D. Lundquist, and M. D. Dettinger, 2008: Meteorological characteristics and overland precipitation impacts of atmospheric rivers affecting the west coast of North America based on eight years of SSM/I satellite observations. *J. Hydrometeor.*, **9**, 22–47, https://doi.org/10.1175/2007JHM855.1.

——, M. Hughes, B. J. Moore, F. M. Ralph, and E. M. Sukovich, 2013: Sierra barrier jets, atmospheric rivers, and precipitation characteristics in Northern California: A composite perspective based on a network of wind profilers. *Mon. Wea. Rev.*, **141**, 4211–4233, https://doi.org/10.1175/MWR-D-13-00112.1.

Newell, R. E., N. E. Newell, Y. Zhu, and C. Scott, 1992: Tropospheric rivers?—A pilot study. *Geophys. Res. Lett.*, **19**, 2401–2404, https://doi.org/10.1029/92GL02916.

Pereira, S., A. M. Ramos, J. L. Zêzere, R. M. Trigo, and J. M. Vaquero, 2016: Spatial impact and triggering conditions of the exceptional hydro-geomorphological event of December 1909 in Iberia. *Nat. Hazards Earth Syst. Sci.*, **16**, 371–390, https://doi.org/10.5194/nhess-16-371-2016.

Philippon, N., M. Rouault, Y. Richard, and A. Favre, 2012: The influence of ENSO on winter rainfall in South Africa. *Int. J. Climatol.*, **32**, 2333–2347, https://doi.org/10.1002/joc.3403.

Ralph, F. M., and M. D. Dettinger, 2012: Historical and national perspectives on extreme West Coast precipitation associated with atmospheric rivers during December 2010. *Bull. Amer. Meteor. Soc.*, **93**, 783–790, https://doi.org/10.1175/BAMS-D-11-00188.1.

——, P. J. Neiman, and G. A. Wick, 2004: Satellite and CALJET aircraft observations of atmospheric rivers over the eastern North Pacific Ocean during the winter of 1997/98. *Mon. Wea. Rev.*, **132**, 1721–1745, https://doi.org/10.1175/1520-0493(2004)132<1721:SACAOO>2.0.CO;2.

——, ——, ——, S. I. Gutman, M. D. Dettinger, D. R. Cayan, and A. B. White, 2006: Flooding on California's Russian River: Role of atmospheric rivers. *Geophys. Res. Lett.*, **33**, L13801, https://doi.org/10.1029/2006GL026689.

——, T. Coleman, P. J. Neiman, R. J. Zamora, and M. D. Dettinger, 2013: Observed impacts of duration and seasonality of atmospheric-river landfalls on soil moisture and runoff in coastal Northern California. *J. Hydrometeor.*, **14**, 443–459, https://doi.org/10.1175/JHM-D-12-076.1.

Ramos, A. M., R. M. Trigo, and M. L. R. Liberato, 2014: A ranking of high-resolution daily precipitation extreme events for the Iberian Peninsula. *Atmos. Sci. Lett.*, **15**, 328–334, https://doi.org/10.1002/asl2.507.

——, ——, ——, and R. Tomé, 2015: Daily precipitation extreme events in the Iberian Peninsula and its association with atmospheric rivers. *J. Hydrometeor.*, **16**, 579–597, https://doi.org/10.1175/JHM-D-14-0103.1.

——, R. Nieto, R. Tomé, L. Gimeno, R. M. Trigo, M. L. R. Liberato, and D. A. Lavers, 2016: Atmospheric rivers moisture sources from a Lagrangian perspective. *Earth Syst. Dyn.*, **7**, 371–384, https://doi.org/10.5194/esd-7-371-2016.

Reason, C. J. C., 1998: Warm and cold events in the southeast Atlantic/southwest Indian Ocean region and potential impacts on circulation and rainfall over southern Africa. *Meteor. Atmos. Phys.*, **69**, 49–65, https://doi.org/10.1007/BF01025183.

——, and D. Jagadheesha, 2005: Relationships between South Atlantic SST variability and atmospheric circulation over the South African region during austral winter. *J. Climate*, **18**, 3339–3355, https://doi.org/10.1175/JCLI3474.1.

——, and M. Rouault, 2005: Links between the Antarctic Oscillation and winter rainfall over western South Africa. *Geophys. Res. Lett.*, **32**, L07705, https://doi.org/10.1029/2005GL022419.

——, ——, J. L. Melice, and D. Jagadheesha, 2002: Interannual winter rainfall variability in SW South Africa and large scale ocean–atmosphere interactions. *Meteor. Atmos. Phys.*, **80**, 19–29, https://doi.org/10.1007/s007030200011.

Rienecker, M. M., and Coauthors, 2011: MERRA: NASA's Modern-Era Retrospective Analysis for Research and Applications. *J. Climate*, **24**, 3624–3648, https://doi.org/10.1175/JCLI-D-11-00015.1.

Rutz, J. J., and W. J. Steenburgh, 2012: Quantifying the role of atmospheric rivers in the interior western United States. *Atmos. Sci. Lett.*, **13**, 257–261, https://doi.org/10.1002/asl.392.

——, ——, and F. M. Ralph, 2014: Climatological characteristics of atmospheric rivers and their inland penetration over the western United States. *Mon. Wea. Rev.*, **142**, 905–921, https://doi.org/10.1175/MWR-D-13-00168.1.

Singleton, A. T., and C. J. C. Reason, 2007a: A numerical model study of an intense cutoff low pressure system over South Africa. *Mon. Wea. Rev.*, **135**, 1128–1150, https://doi.org/10.1175/MWR3311.1.

——, and ——, 2007b: Variability in the characteristics of cut-off low pressure systems over subtropical southern Africa. *Int. J. Climatol.*, **27**, 295–310, https://doi.org/10.1002/joc.1399.

Sun, X., K. H. Cook, and E. K. Vizy, 2017: The South Atlantic subtropical high: Climatology and interannual variability. *J. Climate*, **30**, 3279–3296, https://doi.org/10.1175/JCLI-D-16-0705.1.

Tennant, W., 2004: Considerations when using pre-1979 NCEP/NCAR reanalyses in the Southern Hemisphere. *Geophys. Res. Lett.*, **31**, L11112, https://doi.org/10.1029/2004GL019751.

Trenberth, K. E., J. T. Fasullo, and J. Mackaro, 2011: Atmospheric moisture transports from ocean to land and global energy flows in reanalyses. *J. Climate*, **24**, 4907–4924, https://doi.org/10.1175/2011JCLI4171.1.

Viale, M., and M. N. Nuñez, 2011: Climatology of winter orographic precipitation over the subtropical central Andes and associated synoptic and regional characteristics. *J. Hydrometeor.*, **12**, 481–507, https://doi.org/10.1175/2010JHM1284.1.

Warner, M. D., C. F. Mass, and E. P. Salathé, 2012: Wintertime extreme precipitation events along the Pacific Northwest coast: Climatology and synoptic evolution. *Mon. Wea. Rev.*, **140**, 2021–2043, https://doi.org/10.1175/MWR-D-11-00197.1.

Wick, G. A., P. J. Neiman, F. M. Ralph, and T. M. Hamill, 2013: Evaluation of forecasts of the water vapor signature of atmospheric rivers in operational numerical weather prediction models. *Wea. Forecasting*, **28**, 1337–1352, https://doi.org/10.1175/WAF-D-13-00025.1.

WWF, 2013: An introduction to South Africa's water source areas. World Wildlife Fund South Africa (WWF-SA) Rep., 29 pp.

Zhu, Y., and R. E. Newell, 1998: A proposed algorithm for moisture fluxes from atmospheric rivers. *Mon. Wea. Rev.*, **126**, 725–735, https://doi.org/10.1175/1520-0493(1998)126<0725:APAFMF>2.0.CO;2.